Master Thesis

Ab Initio Modelling of Zirconium Hydrides

Johan Olofsson

Master Thesis at Applied Physics 2011

Abstract

Zirconium alloys are very suitable as fuel claddings and structural components in nuclear reactors due to their low cross section for absorption of thermal neutrons and high resistance to corrosion and irradiation damage. Zirconium alloys are however susceptible to hydrogen embrittlement. Precipitation of zirconium hydrides is attributed to the embrittlement effect in zirconium alloys. In this project ab-initio simulations of αZr and the three different zirconium hydrides γ-ZrH, δ-$ZrH_{1.5}$ and ϵ-ZrH_2 are performed to calculate structural, elastic and thermal properties of these different compounds. The goal with the project was to calculate the equilibrium structures of the H-Zr system using ab-initio methods. The results from the calculations of thermal and mechanical properties were found to be in good agreement with previous results and experiments where these were available. Calculations of the phonon band structure for the different hydrides show that the band structure of the hydrides has two characteristic bands, one corresponding to vibrations in the zirconium sublattice and one corresponding to vibrations in the hydrogen sublattice. The calculated heat capacity of the different compounds was found to be described very well by the Einstein model for the heat capacity of a solid. By calculating the free energy of formation for the different compounds it was found that at high hydrogen concentrations ϵ-hydride is the equilibrium structure. At intermediate hydrogen levels the equilibrium structure can't be determined.

Contents

1 Introduction **1**

2 Background **2**
2.1 Fuel cladding 2
2.1.1 Reactivity inserted accidents 2
2.1.2 Degradation of fuel claddings inside the reactor 3
2.2 Hydrogen Embrittlement 3
2.2.1 The Zirconium-Hydrogen binary system 3
2.2.2 Hydride precipitation 5
2.2.3 Macroscopic Embrittlement 6
2.2.4 Delayed Hydrogen Cracking 6

3 Computational Methods **6**
3.1 Density Functional Theory 6
3.1.1 Exchange Correlation Functionals 8
3.2 Phonon calculations 9
3.2.1 The small displacement method for calculating phonon dispersion curves 10

4 Objective **11**

5 Calculations **11**
5.1 Equilibrium structures 11
5.2 Elastic constants 12
5.3 Thermal properties 13

6 Results **15**
6.1 Equilibrium structures and mechanical properties 15
6.2 Thermal properties 17

7 Discussion **23**

8 Conclusion and outlook **26**

Acknowledgement **27**

References **28**

1 Introduction

To meet the increasing demand for energy in the world today, nuclear power has had a renaissance in later years as new reactors are being built and planned and already running reactors are given prolonged lifetimes.

Due to the severe consequences that can result from an accident in a nuclear power plant, security aspects have always been in focus in the design and operation of nuclear reactors. To protect the staff at the power plants and the people and environment around the plants from radioactivity and prevent leakage from the core, several barriers are placed between the fuel itself and the surroundings. The first barrier that isolates the fuel is the fuel cladding.

During operation of a nuclear reactor the fuel cladding will degrade due to corrosion, irradiation and hydrogen uptake, which can cause the cladding material to fracture if a high mechanical stress is applied.

Today zirconium alloys are the primary material used for fuel claddings and structural components in nuclear power plant applications[1]. Zirconium is well suited for nuclear applications since it has a low cross section for absorbing thermal neutrons and a high resistance to corrosion and irradiation damage. However, zirconium and zirconium alloys have shown to be susceptible to degradation from hydrogen uptake, a phenomenon commonly known as hydrogen embrittlement[2].

2 Background

In this section, a brief introduction to nuclear fuel claddings and hydrogen embrittlement will be presented. Since the subject of this thesis is ab-initio modelling of zirconium hydrides the focus has been placed in the phenomenon of hydrogen embrittlement in zirconium.

2.1 Fuel cladding

Most of the nuclear reactors in operation today are light water moderated reactors (LWR). They consists primarily of two types, the first one is the boiling water reactor (BWR), where the heat generated in the core is used to transform water into steam that is then used to generate electricity through steam turbines. The second type of LWR:s is the pressurized water reactor (PWR) where the coolant is held at a high pressure to prevent it from boiling and steam is generated in a secondary loop.

The nuclear fuel in LWR:s consists of ceramic uranium dioxide, which is pressed into pellets and placed in cylindrical tubes, about 1 cm in diameter, where the gap between the pellets and the cladding is filled with helium to increase the heat conduction between the fuel and cladding. These fuel rods, is then bundled together to form a fuel bundle.

The cladding serves as a barrier that prevents radioactive fission products to enter the coolant and therefore it is important that the cladding has an high resistance to corrosion and irradiation damage. Zirconium alloys such as Zircaloy or Zirlo are today the materials used for fuel claddings. These alloys consists mainly of zirconium, but also small amounts of niobium, tin, iron, chromium, nickel and some other metals are added to increase the mechanical stability and corrosion resistance[3].

2.1.1 Reactivity inserted accidents

During the operation of a nuclear reactor, a reactivity inserted accident (RIA), such as a sudden control rod withdrawal can occur. During such an accident the reactivity (i.e. fission rate) in the core will increase, causing the temperature of the fuel to increase which in turn will lead to thermal expansion of the fuel and a release of fission gas. The rapid expansion of the fuel and the release of fission gas will cause the pellet to come into contact with the fuel cladding resulting in a pellet-cladding interaction (PCI) which will impose a mechanical load on the cladding since the fuel pellet will expand faster than the cladding. If the mechanical properties of the cladding has been degraded due to corrosion, irradiation or hydrogen uptake, this load

can cause the cladding to break, leading to a release of fission gas and other radioactive particles.

2.1.2 Degradation of fuel claddings inside the reactor

During operation of a nuclear reactor, the alloys used as fuel claddings and structural components will degrade due to irradiation, corrosion and hydrogen uptake. All these processes have the possibility to reduce the mechanical strength and ductility of the alloy[4].

The Zirconium alloys used as cladding materials in most of the modern LWR:s have a high resistance to corrosion and irradiation damage, however, zirconium alloys have been shown to be susceptible to hydrogen embrittlement which can cause the cladding to crack if subject to high stress.

2.2 Hydrogen Embrittlement

It is well established that hydrogen reduces the mechanical strength of metals, a phenomena known since the beginning of the 20th century. It has been known since the 1920s that hydrogen considerable lowers the ductility of metals[5], a phenomena called hydrogen embrittlement.

Hydrogen embrittlement in zirconium and zirconium alloys has been observed since the 1950s[6]. Since α-zirconium has a low solubility for hydrogen, hydride precipitates are attributed to this embrittlement effect. In zirconium alloys hydrogen can produce macroscopic embrittlement in the cladding as well as cause fractures through a process known as Delayed Hydrogen Cracking (DHC)[1][7]. To fully understand the effect of hydrogen in zirconium fuel claddings, the properties of the different hydrides in the zirconium-hydrogen binary system must be reviewed.

2.2.1 The Zirconium-Hydrogen binary system

The zirconium-hydrogen system has been studied extensively throughout the years, which gave Zuzek *et al.* the possibility to construct the phase diagram of the Zr-H system in 1990[8]. Zuzek identifies five different crystal structures in the system: α-Zr, β-Zr, ϵ-ZrH_x, δ-ZrH_x and γ-ZrH_x.

α-Zr has a close-packed hexagonal structure with a low solubility of hydrogen, and is the also the structure of pure zirconium. The terminal solubility of hydrogen in α-Zr decreases fast with temperature, from 6 at.% at 550 °C to less then 0.1 at. % at room temperature[8].

β-Zr is a high temperature phase in the zirconium-hydrogen system, that exist at temperatures above 550 °C. β-Zr has a bcc structure with a high

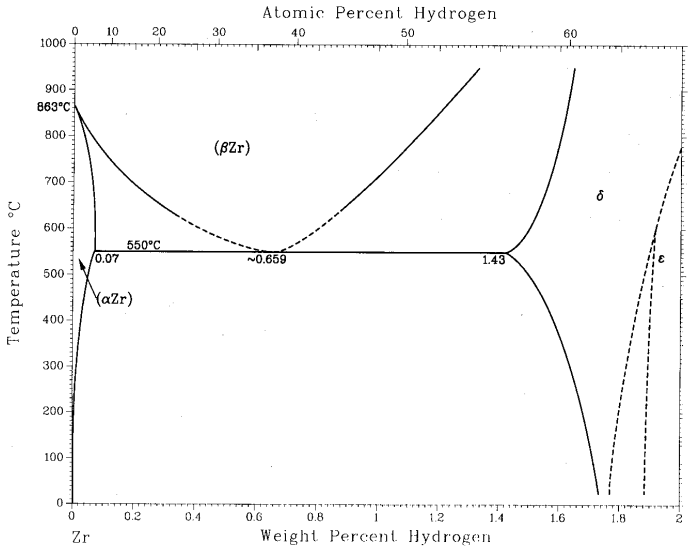

Figure 1: *The phase diagram for the Zr-H system as presented by Zuzek[8]. Note that the γ-ZrH hydride hasn't been included in this phase diagram.*

solubility of hydrogen, up to 54.55 at.% hydrogen can be absorbed in this structure[8].

δ-ZrH_x is a hydride phase with an fcc-structure where the hydrogen atoms occupy random tetrahedral sites in the zirconium lattice. The δ-phase can have a composition of 56.71 to 66.67 at.% hydrogen depending on the temperature, corresponding to a value of $x \approx 1.3-2$, but at temperatures relevant in nuclear reactor applications (up to 400 °C), δ-hydride has a hydrogen content corresponding to $x \approx 1.5 - 1.7$.

At high hydrogen levels ϵ-ZrH_x is formed. This phase has an face-centred tetragonal structure with $c/a < 1$ and hydrogen atoms occupying tetrahedral sites in the lattice. The hydrogen content in the ϵ-hydride corresponds to a value of $x > 1.8$.

There also exists a highly ordered metastable phase called γ-ZrH in the Zr-H system. γ-ZrH has a face centred tetragonal structure with hydrogen atoms occupying tetragonal sites in alternating (110) planes[8]. Because of the highly ordered structure, the hydrogen composition in the γ-hydride is exactly 50 at.%.

The exact nature of when the γ-hydride is observed is still not entirely clear. Small *et al.* observed that in a Zr-2.5Nb alloy, a transformation from δ to γ-hydride took place when cooled below 180 °C [9], indicating that at low temperatures γ-hydride is a equilibrium structure[8].

In figure 1 the phase diagram presented by Zuzek et al [8] is shown. In this diagram the γ-hydride hasn't been included, because of the uncertainty in it's place in the phase diagram. In this figure there are several parts that hasn't been labelled, in these regions the equilibrium structure isn't a pure phase but rather a combination of different phases. There are two unlabelled regions of this phase diagram that are of interest for applications as nuclear fuel claddings. The large unlabelled region below 550° C and with hydrogen concentrations between 0 and 1.7 wt.% H is a region where the equilibrium phase is a combination of αZr, δ-hydride and γ-hydride. Between the equilibrium regions of δ and ϵ-hydride another two-phase region is located. In this region the equilibrium phase is a mixture of δ- and ϵ-hydride.

2.2.2 Hydride precipitation

During operation of a nuclear reactor, the zirconium fuel cladding will oxidise due to the water on the outside of the cladding. In the oxidation process hydrogen is released and some of this will be absorbed in the cladding. However, the exact way that hydrogen is transported through the oxide layer into the zirconium matrix is today not fully understood.

Since αZr has such a low solubility of hydrogen, brittle hydride precipitates will be formed in the cladding. These precipitates have been known to be the cause of hydrogen embrittlement in zirconium since the 1960s[5]. Zirconium hydrides will precipitate as plates, both between and inside the zirconium grains (intra- and inter-granular hydrides) and the orientation of these hydrides will to a great extent affect the impact the hydrides has on the mechanical properties of the zirconium cladding.

Hydrides oriented in the radial direction of the cladding can seriously reduce the mechanical strength of the cladding, since cracks initiated in a radial hydride can grow rapidly, causing the entire cladding to fail, if a sufficient mechanical load is applied. Hydrides oriented in the circumferential (hoop) direction are less likely to cause a complete failure of the cladding.

Precipitation of hydrides in zirconium alloys is a very complex process, and the effects of grain size, applied and residual stresses and many other factors have been extensively investigated. One example is that during the application of a stress, hydrides tend to precipitate perpendicular to the stress axis[2]. Therefore compressive radial strains are often introduced during the manufacturing process of fuel claddings to prevent the formation of radial hydrides. Because of this, the hydrides formed in the cladding have mostly a circumferential orientation and are highly concentrated towards the outside of the cladding due to the steep temperature gradient in the cladding during the operation of the reactor. This is especially evident in high-burnup fuel

rods, where experiments have shown that a dense hydride rim is formed at the outer surface of the cladding.

2.2.3 Macroscopic Embrittlement

As mentioned before, hydrogen absorbed in the cladding will decrease the mechanical strength of the cladding and make it likely to break if a sufficient load is applied to the cladding.

Bai *et al* have shown that in zircaloy-4, a zirconium alloy commonly used as nuclear fuel cladding, there is a change in fracture type when the hydrogen concentration is increased in the material[10]. At low hydrogen concentrations, the fracture was of ductile type, while at higher hydrogen concentrations the fracture was of brittle nature.

2.2.4 Delayed Hydrogen Cracking

In addition to macroscopic hydrogen embrittlement of zirconium, hydrogen can cause the zirconium cladding to fail due to a slow time-dependent crack growth process called delayed hydrogen cracking or delayed hydride cracking (DHC). DHC has been responsible for several failures in different components present in nuclear reactors. Among other things, a DHC-like process has been identified as the reason for radial cracking in BWR fuel claddings[1].

DHC is a step-wise process that starts with hydrogen that diffuses towards the high stress region around a crack tip. When the hydrogen concentration is sufficiently high, hydrides nucleate and grow and then fracture, causing the crack to grow and the process to repeat itself.

3 Computational Methods

In this section, a short introduction to the computational methods used in this thesis will be presented. Density Functional Theory (DFT) is used to calculate the equilibrium structure and mechanical related properties of the different compounds. The thermal properties of the different compounds are calculated using phonon calculations and a technique called the small displacement method.

3.1 Density Functional Theory

In condensed matter physics, knowledge of the electronic structure is the key to find the physical properties of solids. Today DFT is the most popular method used to perform ab initio electronic structure calculations for solids,

mainly because it offers high accuracy in the results while maintaining a reasonably computational cost.

To find the electronic structure of an atom, molecule or solid we most solve the many-body Schroedinger equation, which in the case of N electrons in an external potential will take the form:

$$\left[\sum_{i}^{N}\left(-\frac{1}{2}\nabla_i^2 + V_{ext}(\mathbf{r}_i)\right) + \frac{1}{2}\sum_{i\neq j}\frac{1}{|r_i - r_j|}\right]\Phi(\mathbf{r}_1,...,\mathbf{r}_N) = E\Phi(\mathbf{r}_1,...,\mathbf{r}_N) \tag{1}$$

Here we have used atomic units ($\hbar = e = m_e = 1$) to simplify the expressions. In principle we can solve this equation and from its solutions determine the electronic structure of the system we are interested in.

From a practical point of view, this approach is possible if we are considering small systems but as the number of electrons in the system is increased the computational cost will also increase, making it practically impossible to solve systems with more then a few electrons.

The theoretical foundation for density functional theory was laid in 1964 by Hohenberg and Kohn. They proved that the ground state electron density uniquely determines all the properties of the system, including the many-electron wave-function. At the same time they also proved that for a many-electron system in an external potential the total energy of the system is an unique functional of the density:

$$E[n(\mathbf{r})] = F[n(\mathbf{r})] + \int d\mathbf{r} V_{ext}(\mathbf{r})n(\mathbf{r}) \tag{2}$$

this functional $E[n(\mathbf{r})]$ is furthermore minimized by the ground state electron density $n_0(\mathbf{r})$. The functional $F[n]$ is universal and the same for all systems. Therefore, once this functional is determined the ground-state density and energy of a system can be calculated by minimizing the functional $E[n(\mathbf{r})]$ with respect to the density $n(\mathbf{r})$.

This theoretical framework made it possible for Kohn and Sham to in 1965 formulate a scheme to perform DFT calculations. In this approach the Kohn-Sham functional $E^{KS}[n(\mathbf{r})]$ is used to calculate the total energy of the system:

$$E^{KS}[n(\mathbf{r})] = T_s[n(\mathbf{r})] + E_H[n(\mathbf{r})] + E_{xc}[n(\mathbf{r})] + \int d\mathbf{r} V_{ext}(\mathbf{r})n(\mathbf{r}) \tag{3}$$

Here $T_s[n(\mathbf{r})]$ is the kinetic energy for a system of non interacting electrons, $E_H[n(\mathbf{r})]$ describes the electrostatic interaction energy of the electrons (the Hartree energy) and $E_{xc}[n(\mathbf{r})]$ is called the exchange-correlation energy functional, which incorporates all complicated many-body effects.

The electron density is calculated by replacing the system of N interacting electrons in an external potential with a system of N non-interacting electrons in an effective potential:

$$\left[-\frac{1}{2}\nabla^2 + V_{eff}(\mathbf{r})\right]\phi_i(\mathbf{r}) = \left[-\frac{1}{2}\nabla^2 + V_H(\mathbf{r}) + V_{xc}(\mathbf{r}) + V_{ext}(\mathbf{r})\right]\phi_i(\mathbf{r}) = \epsilon_i\phi_i(\mathbf{r}) \tag{4}$$

In this equation V_H and V_{xc} are the respective functional derivates of the Hartree and exchange correlation energy. The electron density of the system of interacting electrons is then calculated from the Kohn-Sham wave functions through:

$$n(\mathbf{r}) = \sum_i^N |\phi_i(\mathbf{r})|^2 \tag{5}$$

From all this we see that the effective potential in the Kohn-Sham equations depends on the total electron density, which in turn depends on the effective potential itself. Therefore the Kohn-Sham equations must be solved through a iterative self-consistency cycle.

3.1.1 Exchange Correlation Functionals

The difficulty with the DFT formalism presented above is to find a sufficiently accurate description of the exchange-correlation functional. The other terms in the Kohn-Sham functional (Eq. (3)) can be exactly described but when it comes to the exchange correlation functional, approximations are necessary.

Historically, the most used approximation for the exchange-correlation functional, is the Local Density Approximation (LDA). In this approximation, the starting point is the homogeneous electron gas. In a homogeneous electron gas the exchange energy can be calculated exactly and the correlation energy can be calculated using parametrizations of data from very precise Quantum Monte Carlo simulations. In the Local Density Approximation, the exchange-correlation, E_{xc}, is expressed as:

$$E_{xc}[n] = \int d\mathbf{r}\epsilon_{xc}(n(\mathbf{r})) \tag{6}$$

where $\epsilon_{xc}(n)$ is the exchange-correlation energy density for a homogeneous electron gas with density n. Despite this rather crude approximation the LDA approach has been successfully used to calculate electronic properties of a large number of systems. Some of its success can be explained by the fact that in many metals, the electron gas is similar to a homogeneous electron gas. However, LDA also gives accurate results for systems which have a electron

structure far from that of a homogeneous electron gas. This can in part be explained by the fact that LDA systematically overestimates the exchange energy and at the same time underestimates the correlation energy, causing the errors to cancel each other out to a large extent, resulting in surprisingly good results for E_{xc}.

In order to improve the exchange correlation functional and include some non-local effects, not only the local density but also the gradients of the local density can be used to calculate E_{xc}. There exists many ways to include gradients in the calculation of E_{xc} but today functionals of the general form

$$E_{xc}[n] = \int d\mathbf{r} f(n(\mathbf{r}),\nabla n(\mathbf{r})) \tag{7}$$

is often used. These functionals is known as Generalized Gradient Approximations or GGA:s. The difference between different GGA functionals is in the choice of the functional f in the above equation and today many different GGA-functionals is being used. For solids the PBE-functional (named after Perdrew, Burke and Ernzerhof[11]) is the most common functional used today. Generalized Gradient Approximations are also known as semi-local approximations in contrast to the local LDA-functional.

Today DFT calculations using GGA to approximate the exchange and correlation energy give reliable results for many different systems and chemical bonds. When it comes to describe weak and long-range interactions like the van der Waals interaction, these effects are not properly included in the LDA or various GGA:s. Much research is being performed in order to find new and improved functionals to describe even these long-range interactions and find a full non-local exchange correlation fuctional.

3.2 Phonon calculations

Density functional theory is very good at determining ground-state properties of materials at $T = 0$ and zero pressure. However, when considering phase stability and thermodynamics of crystalline materials, knowledge of the phonon frequencies is crucial.

When the phonon frequencies of a crystalline material are known we are able to, among other things, calculate the phonon contribution to Helmholtz free energy and the phonon heat capacity.

Methods to calculate the phonon frequencies can be classified into two broad categories, linear response methods and direct methods. In linear response methods the dynamical matrix of the system is expressed in terms of the inverse dielectric matrix.

Direct methods or small-displacement methods to calculate the phonon frequencies come into two variants. The first one, that is called the frozen-phonon method, in which the phonon energy is calculated as a function of displacement amplitude from the difference in total energy between the perturbed and unperturbed lattice. In the second variant of the direct method, the Hellmann-Feynmann theorem is used to calculate the forces on each atom in the lattice. From these forces force constants are calculated and these are in turn used to calculate the dynamical matrix of the system. The phonon dispersion curves can then be calculated from the eigenvalues of the dynamical matrix.[12]

3.2.1 The small displacement method for calculating phonon dispersion curves

By displacing atoms in a periodic lattice, the force on atom s in unit cell ℓ is given by:

$$F_{\ell s\alpha} = -\frac{\partial U}{\partial u_{\ell s\alpha}} = -\sum_{\ell' t\beta} \Phi_{\ell s\alpha,\ell' t\beta} u_{\ell' t\beta} \tag{8}$$

where $u_{\ell' t\beta}$ is the displacement of atom t in unit cell ℓ', $\Phi_{\ell s\alpha,\ell' t\beta}$ is the force constant matrix and α and β denotes the cartesian components, x, y and z.

With knowledge of the force constants, the dynamical matrix, defined as:

$$D_{s\alpha,t\beta}(\mathbf{k}) = \frac{1}{\sqrt{M_s M_t}} \sum_{\ell t\beta} \Phi_{\ell s\alpha,0t\beta} \exp\left[i\mathbf{k}\cdot(\mathbf{R_0} + \tau_\mathbf{t} - \mathbf{R}_\ell - \tau_\mathbf{s})\right] \tag{9}$$

can be calculated. In the above equation $\mathbf{R}_\ell + \tau_s$ represents the equilibrium position of atom s, in unit cell ℓ and with mass M_s. The sum in the above equation runs over all unit cells in the infinite lattice.

The phonon vibrational frequencies $\omega_{\mathbf{k}s}$ is defined as the square root of the eigenvalues to the dynamical matrix, so by knowledge of the force constants, the dynamical matrix and the frequencies can be calculated.

In practical calculations, it is not possible to calculate every force constant needed to calculate the full dynamical matrix. Because of this, in practical calculations a supercell approach is applied. In this approach, it is assumed that atoms that are separated more than a specific distance d are not interacting with each other[13].

4 Objective

As mentioned above, hydrogen embrittlement can cause a macroscopic embrittlement of zirconium alloys, making them extremely brittle and susceptible to fracture. At a macroscopic level this embrittlement effect is quite well understood, however at a microscopic level the exact process is unknown.

A series of TEM (Transmission Electron Microscopy) studies has been performed at Studsvik Nuclear AB on several irradiated fuel claddings. In these studies a difference in the hydrides crystal structure was observed between the samples above the ductile to brittle transition and the samples below this transition.

The objective with this thesis is to, by using ab-initio methods, calculate structural, elastic and thermal properties of the different zirconium hydrides, whereby increasing our understanding of the effects hydrogen has on the mechanical properties of zirconium fuel claddings.

Furthermore, by calculating the free energy of formation for the different hydrides as a function of temperature using ab-initio methods, the equilibrium hydrides at different temperatures and hydrogen concentrations can be determined.

5 Calculations

DFT (Density Functional Theory) calculations are performed using the GPAW-code[14] and the ASE-interface[15]. The GPAW-code implements the projector-augmented wave (PAW) formalism using real-space grids to represent wave functions, pseudo electron densities and potentials. In these calculations the Perdew-Burke-Ernzerhof (PBE) exchange-correlation functional[11], a real-space grid spacing of h=0.15 Å and a Monkhorst-Pack k-point sampling[16] with 6x6x6 k-points are used.

The grid-spacing and number of k-points used in the calculations were chosen to ensure that the total energy was sufficiently converged. By increasing the number of k-points or decreasing the grid-spacing the total energy in the calculations was seen to change with at most 0.05 eV.

5.1 Equilibrium structures

The equilibrium lattice parameters for αZr and the different hydrides are determined by relaxation of atomic structure and calculation of the total energy of the compound in question for different values of the lattice parameters. A

Table 1: *The different deformations used to calculate the elastic constants of the different compounds*

Deformation	strains (unlisted $e_i = 0$)	$\Delta E/V_0$
ϵ^1	$e_1 = \delta$	$\frac{1}{2}C_{11}\delta^2$
ϵ^2	$e_2 = \delta$	$\frac{1}{2}C_{22}\delta^2$
ϵ^3	$e_3 = \delta$	$\frac{1}{2}C_{33}\delta^2$
ϵ^4	$e_1 = e_2 = \delta$	$(\frac{1}{2}C_{11} + \frac{1}{2}C_{22} + C_{12})\delta^2$
ϵ^5	$e_1 = e_3 = \delta$	$(\frac{1}{2}C_{11} + \frac{1}{2}C_{33} + C_{13})\delta^2$
ϵ^6	$e_2 = e_3 = \delta$	$(\frac{1}{2}C_{22} + \frac{1}{2}C_{33} + C_{23})\delta^2$
ϵ^7	$e_4 = \delta$	$\frac{1}{2}C_{44}\delta^2$
ϵ^8	$e_5 = \delta$	$\frac{1}{2}C_{55}\delta^2$
ϵ^9	$e_6 = \delta$	$\frac{1}{2}C_{66}\delta^2$

forth order polynomial is then fitted to the data and the minimum of this polynomial corresponds to the equilibrium lattice parameters.

5.2 Elastic constants

The elastic constants of the different zirconium hydrides are calculated by deforming the bravais lattice, $\mathbf{R}$, of the crystal to a deformed state, $\mathbf{R}'$ according to:

$$\mathbf{R}' = \mathbf{R} \begin{bmatrix} 1 + e_{xx} & \frac{1}{2}e_{xy} & \frac{1}{2}e_{xz} \\ \frac{1}{2}e_{xy} & 1 + e_{yy} & \frac{1}{2}e_{yz} \\ \frac{1}{2}e_{xz} & \frac{1}{2}e_{yz} & 1 + e_{zz} \end{bmatrix} \tag{10}$$

The change in energy of the crystal due to the deformation can be described by the following formula:

$$U = \frac{E - E_0}{V_0} = \frac{1}{2}\sum_{i=1}^{6}\sum_{j=1}^{6} C_{ij}e_i e_j \tag{11}$$

This equation is valid for small strains and the coefficients C_{ij} are the elastic constants of the crystal and e_i and e_j are components of the strain matrix that describes the deformation, where the indices i,j = 1,...,6 correspond to the different strains, i,j = 1,...,6 = xx,yy,zz,yz,xz,yx. In this work nine different deformations were used to calculate the different elastic constants and these deformations are presented in table 1. The same deformations were used for the different hydrides and αZr. The amplitude, δ, of the deformation is varied between -0.015 and 0.015 and by calculating the total energy of the

different compounds as a function of the strain amplitude and fit a parabolic function to the calculated energies the elastic constants C_{ij} are calculated. When the elastic constants of a single crystal for a material is known bulk modulus (B) and shear modulus (G) of the material can be calculated using the Voigt-Reuss-Hill-method[17]. In this method the bulk modulus, B, are estimated by:

$$B = \frac{B_{Voigt} + B_{Reuss}}{2} \tag{12}$$

$$9B_{Voigt} = (C_{11} + C_{22} + C_{33}) + 2(C_{12} + C_{13} + C_{23}) \tag{13}$$

$$\frac{1}{B_{Reuss}} = (S_{11} + S_{22} + S_{33}) + 2(S_{12} + S_{13} + S_{23}) \tag{14}$$

The shear modulus, G, are estimated by:

$$G = \frac{G_{Voigt} + G_{Reuss}}{2} \tag{15}$$

$$15G_{Voigt} = (C_{11} + C_{22} + C_{33}) - (C_{12} + C_{13} + C_{23}) + 3(C_{44} + C_{55} + C_{66}) \tag{16}$$

$$\frac{15}{G_{Reuss}} = 4(S_{11} + S_{22} + S_{33}) - 4(S_{12} + S_{13} + S_{23}) + 3(S_{44} + S_{55} + S_{66}) \tag{17}$$

In these equations S_{ij} are the inverse elastic constants obtained by taking the inverse of the elastic constant matrix C_{ij}.

Young's modulus, E, for different materials can be calculated from the bulk and shear modulus by using the standard formula

$$E = \frac{9BG}{G + 3B} \tag{18}$$

5.3 Thermal properties

The phonon band structure and thermal properties of the different hydrides are calculated using the small displacement method as implemented in the phonopy[18] code. In our calculations, atoms were displaced a distance of 0.01 Å and a super-cell of $2 \times 2 \times 2$ unit cells were used to calculate the phonon band structure for the different hydrides. For αZr a super-cell with $3 \times 3 \times 2$ unit cells and a displacement of 0.01 Å were used. From the phonopy code the phonon contribution to the free energy, entropy and heat capacity of the compounds as a function of temperature is then calculated.

The free energy, $F(T)$, of the different compounds is then evaluated according to the following formula:

$$F(T) = E_{elec} + F_{phonon}(T) \tag{19}$$

Here E_{elec} is the total energy of the compounds equilibrium structure and F_{phonon} is the contribution to the free energy from the phonon vibrations. The enthalpy of the crystal can then be calculated using the relation

$$H(T) = E_{elec} + F_{phonon}(T) + TS_{phonon}(T) \tag{20}$$

Here the contribution to the enthalpy from pressure has been neglected.

To calculate the free energy of formation and enthalpy of formation for the different hydrides the temperature dependence of the enthalpy and free energy of hydrogen gas must also be known, and these properties are calculated using the `thermochemistry`-module in ASE. The `thermochemistry`-module calculates the enthalpy, entropy and free energy of hydrogen gas using a ideal gas approximation. In this approximation the enthalpy of the gas is calculated as an extrapolation from the energy at 0 K, according to the formula:

$$H(T) = E_{elec} + E_{zeropoint} + \int_0^T c_P dT \tag{21}$$

There the first two terms are the electronic energy and zero point vibration energy and the third term is the integral of the constant pressure heat capacity. To calculate the entropy and free energy of hydrogen gas in the ideal gas approximation a reference pressure, P_0, must be specified, and the entropy at an arbitrary pressure can when be calculated as:

$$S(T,P) = S(T,P_0) - k_B \ln\left(\frac{P}{P_0}\right) \tag{22}$$

The free energy of hydrogen gas can then be calculated as

$$\begin{aligned} F_{idealgas}(T,P) &= H(T) - TS(T,P) = \\ &= E_{elec} + E_{zeropoint} + \int_0^T c_P dT - TS(T,P) \end{aligned} \tag{23}$$

The free energy of formation and enthalpy of formation for the different compounds can then be calculated using the following formulas:

$$F_{form,ZrH_x} = F_{ZrH_x} - (F_{\alpha Zr} + \frac{x}{2}F_{H_2}) \tag{24}$$

$$H_{form,ZrH_x} = H_{ZrH_x} - (H_{\alpha Zr} + \frac{x}{2}H_{H_2}) \tag{25}$$

In the calculations performed in this work the reference pressure used are 1 atm (101,3 kPa), and the actual pressure of the hydrogen gas is assumed to also be 1 atm.

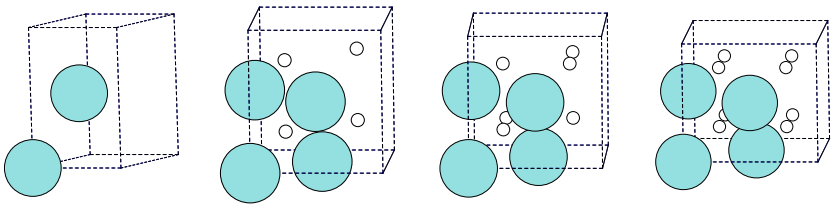

(a) αZr (b) γ-ZrH (c) δ-$ZrH_{1.5}$ (d) ϵ-ZrH_2

Figure 2: *The unit cells for αZr and the different hydrides used in the calculations*

6 Results

In figure 2 the unit cells used in the calculations for αZr and the three different hydrides is presented. As mentioned before, αZr has a hexagonal close-packed structure and the unit cell has a base with two atoms. γ-ZrH has a face-centered tetragonal structure with four hydrogen atoms occupying tetragonal sites in the unit cell. These hydrogen atoms can either have a planar or diamond geometry. However, calculations shows that the diamond geometry has a slightly lower binding energy than the planar geometry and therefore only the planar geometry of the γ-ZrH (figure 2(b)) is considered further on in this work.

In reality the δ-hydride has a fcc-structure with a H/Zr ratio of about 1.66 and hydrogen atoms occupying random tetragonal sites in the zirconium lattice. This non stoichiometric phase is hard to model exactly and therefore a H/Zr ratio of 1.5 was chosen to model the δ-hydride in this work.

The ϵ-hydride has a face-centered tetragonal structure with all tetragonal sites in the unit cell occupied by hydrogen atoms.

6.1 Equilibrium structures and mechanical properties

The resulting equilibrium lattice parameters for the different hydrides and αZr is summarized in table 2 together with experimental data and the results from previous calculations. As seen the results from this study is in good agreement with both experimental results and previous calculations.

The results from the calculation of the elastic constants, bulk modulus and shear modulus of the different hydrides are presented in table 3. From the calculated values of the bulk and shear modulus Youngs modulus of the different hydrides are also calculated.

Table 2: *The resulting equilibrium structures for αZr and the different zirconium hydrides together with experimental data and the results from previous calculations*

	present work		experiment		previous work	
	a	c	a	c	a	c
αZr	3.237	5.157	3.232[1]	5.147[1]	3.223[2]	5.175[2]
			3.232[3]	5.148[3]	3.23[4]	5.18[4]
γZrH	4.592	4.998	4.596[3]	4.969[3]	4.586[2]	4.98[2]
					4.58[4]	5.04[4]
$\delta ZrH_{1.5}$	4.775	-	4.771[1]	-	4.67[2]	-
					4.79[4]	-
ϵZrH_2	4.999	4.433	4.975[3]	4.451[3]	4.72[2]	4.21[2]
			4.975[5]	4.47[5]	5.01[4]	4.44[4]

[1] Reference [19], [2] Reference [20], [3] Reference [8],
[4] Reference [21], [5] Reference [22]

Table 3: *Calculated elastic constants (C_{ij}), Bulk modulus (B), shear modulus (G), and Youngs modulus (E)for the different hydrides, everything in units of GPa. Comparison with experiments and previous calculations is presented if available*

	C_{11}	C_{22}	C_{33}	C_{12}	C_{13}	C_{23}	C_{44}	C_{55}	C_{66}	B	G	E
αZr	159	159	155	42	68	68	26	26	50	92	38	100
	142[1]		164[1]		64[1]		29[1]		39[1]	92[1]		
	155[2]		173[2]	65[2]	67[2]		36[2]		97[2]			
γ-ZrH	132	132	169	119	95	95	62	62	19	117	35	96
	128[3]		187[3]	126[3]	70[3]		55[3]		66[3]	117[3]	44[3]	117[3]
δ-$ZrH_{1.5}$	108	108	108	139	139	139	51	51	51	128	24	69
	63[3]		65[3]	28[3]	44[3]		93[3]		101[3]	47[3]	63[3]	130[3]
ϵ-ZrH_2	159	159	137	143	103	103	48	48	66	125	31	86
	102[3]	103[3]	108[3]	20[3]	11[3]	12[3]	36[3]	36[3]	24[3]	44[3]	37[3]	87[3]
	166[4]		146[4]	141[4]	107[4]		31[4]		61[4]	130[4]	29[4]	80[4]

[1] Reference [21], [2] Reference [23], [3] Reference [20], [4] Reference [24]

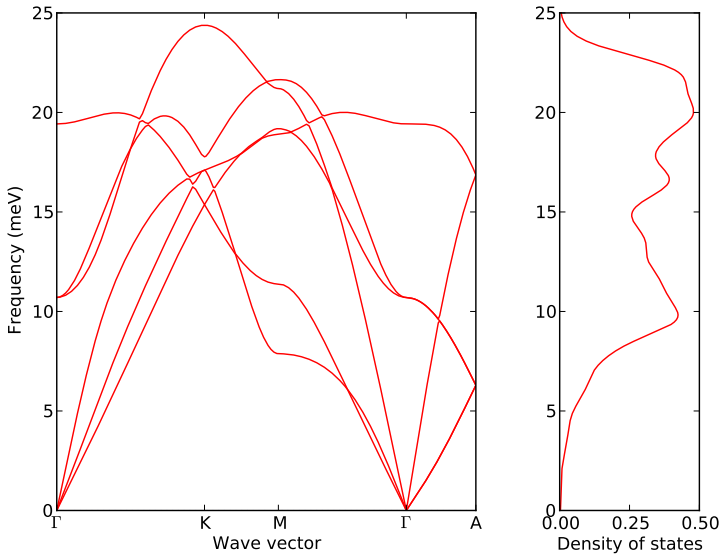

Figure 3: *The phonon band structure and density of states for αZr*

6.2 Thermal properties

In figures 3-6 the phonon band structure along the high symmetry lines together with the phonon density of states for αZr and the different hydrides can be seen.

The phonon band structure for αZr was calculated using the primitive unit cell, consisting of two Zr atoms, and hence six phonon bands can be seen. The primitive unit, consisting of one Zr and two H atoms was also used when calculating the phonon band structure for ϵ-hydride. In the case of the γ-hydride a unit cell consisting of two Zr and two H atoms was used and in the case of the δ-hydride a unit cell consisting of four Zr and six H atoms was used.

With knowledge of the phonon dispersion relations, the phonon contributions to the free energy and the heat capacity of the different hydrides can be calculated.

In figure 7, 8, 9 and 10 the calculated heat capacity, free energy of formation, enthalpy and enthalpy of formation for αZr and the three different hydrides are shown as a function of temperature.

In table 4 the formation energy of the different hydrides at $T = 0K$ is presented.

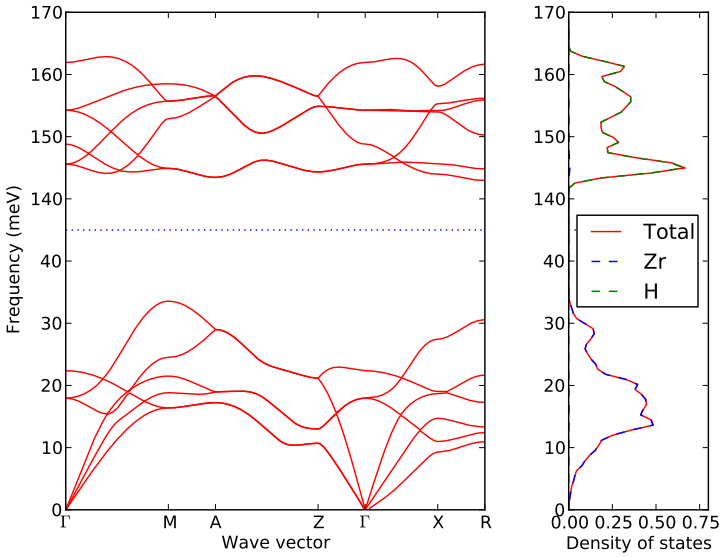

Figure 4: *The phonon band structure and the corresponding total density of states (DOS) and partial density of states (PDOS) for γZrH. The PDOS describes the contribution to the total DOS from the different atoms.*

Table 4: *Formation energy for the different zirconium hydrides at T=0 K, in units of eV. The first value is the formation energy when only the electronic energy are taken into account, the second value is the formation energy when the contribution from zero-point vibrations are also taken into account*

	ΔE_{elec}	$\Delta E_{elec+vib}$
γ-ZrH	-1.19	-0.76
δ-$ZrH_{1.5}$	-1.75	-1.12
ϵ-ZrH_2	-2.36	-1.53

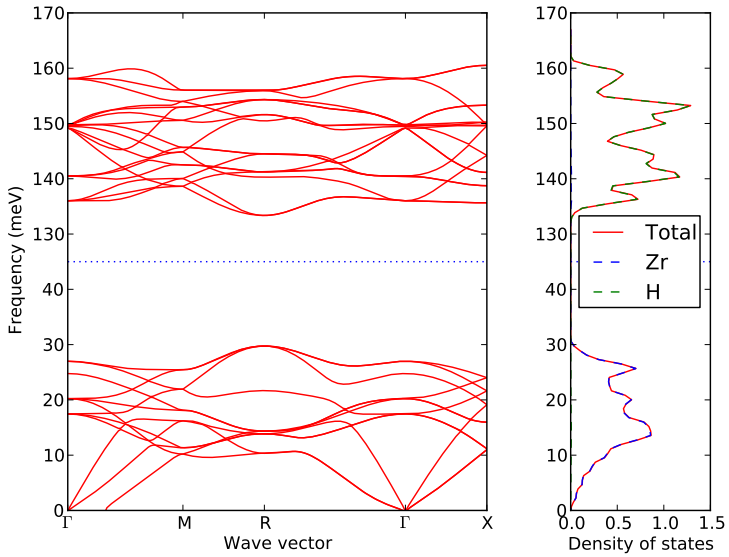

Figure 5: *The phonon band structure and the corresponding total density of states (DOS) and partial density of states (PDOS) for $\delta ZrH_1.5$. The PDOS describes the contribution to the total DOS from the different atoms.*

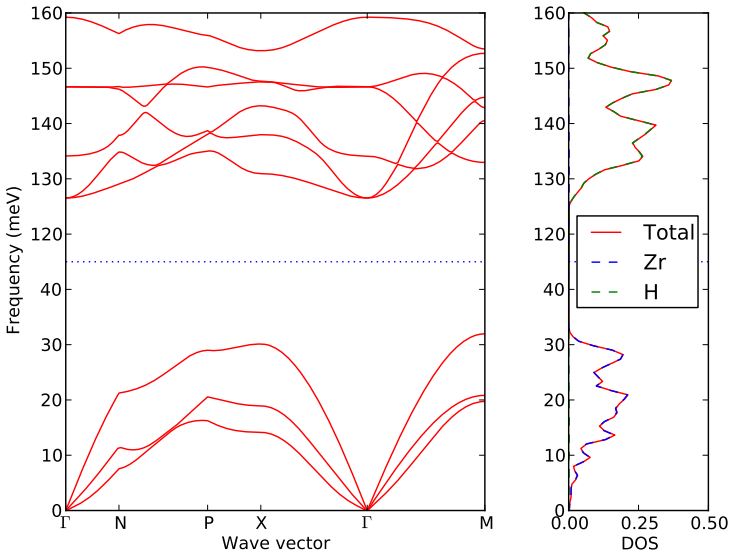

Figure 6: *The phonon band structure and the corresponding total density of states (DOS) and partial density of states (PDOS) for ϵZrH_2. The PDOS describes the contribution to the total DOS from the different atoms.*

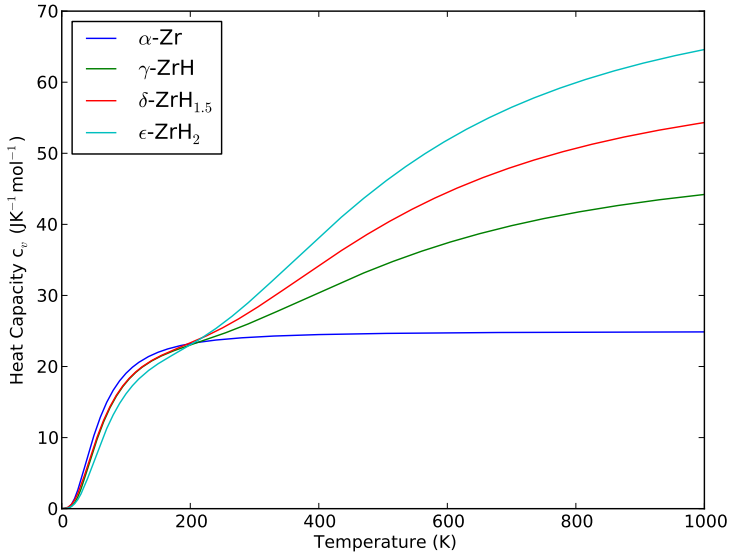

Figure 7: *The calculated heat capacity for αZr and the three different hydrides*

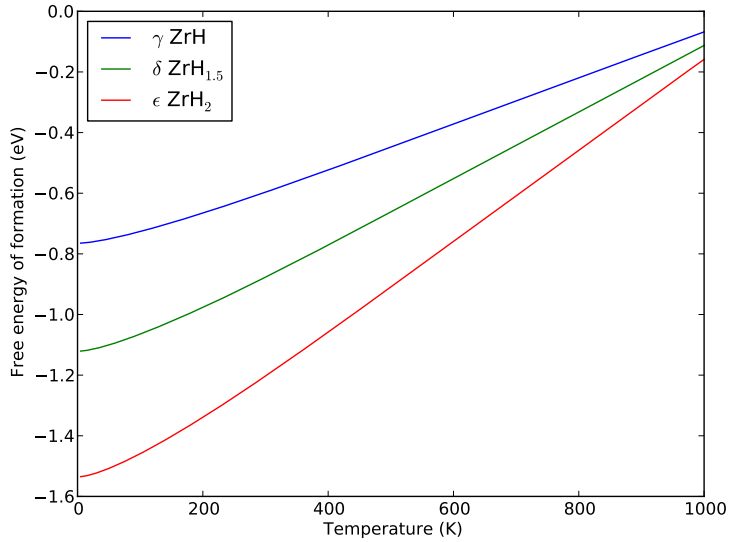

Figure 8: *The calculated free energy of formation for the different hydrides relative regular αZr and hydrogen gas, H_2.*

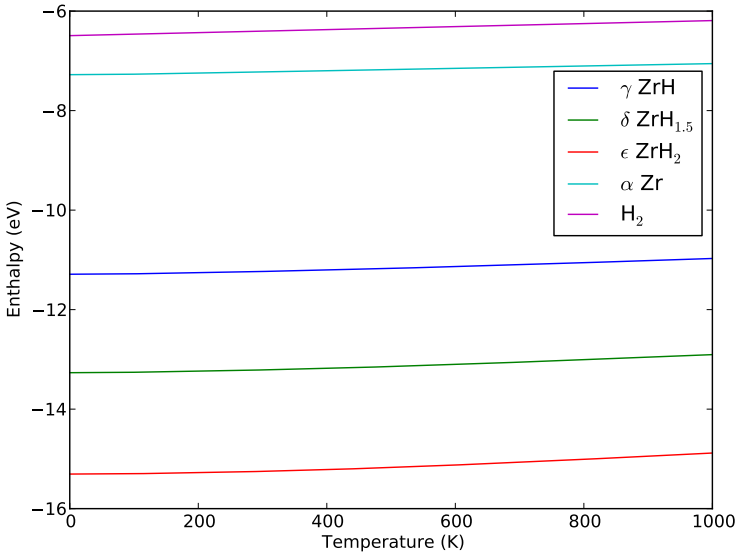

Figure 9: *The calculated temperature dependence of the enthalpy for hydrogen gas, αZr and the three different hydrides*

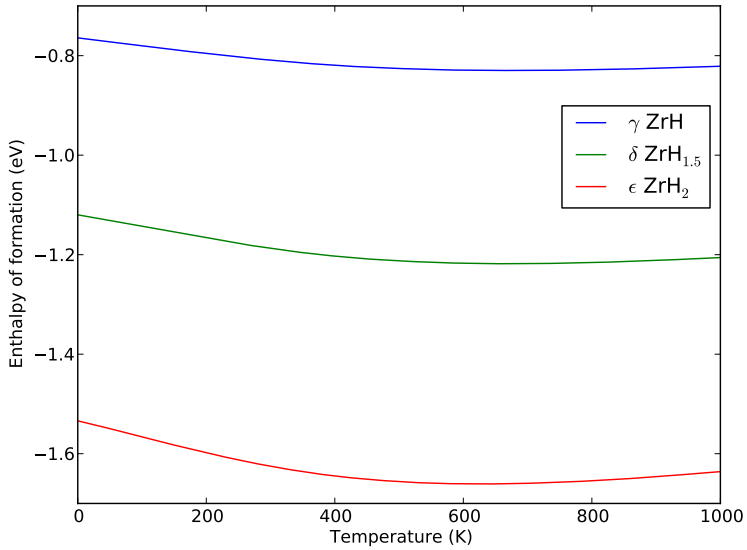

Figure 10: *The enthalpy of formation for the three different zirconium hydrides considered in this work. The enthalpy of formation is calculated using a system of hydrogen gas and αZr as reference system.*

7 Discussion

As seen in table 2 the lattice parameters calculated in this work are in good agreement with both experimental data and previous calculations. This is not very surprising and shows the great strength and accuracy of the ab-initio methods used in these calculations.

When we take a closer look on the calculated elastic constants for the different hydrides we see a clear difference in our results compared to the results of Zhu et al[20]. However, Zhang et al [24] has also calculated the elastic constants of the ϵ-ZrH_2 hydride and their results are in good agreement with our calculated results.

When studying the calculated values for the elastic constants of αZr there is a difference between the values calculated in this thesis and those of previous calculations and experimental values. The source of this difference is not known at the present, but it is worth noting that the calculated values for the bulk modulus, shear modulus and Youngs modulus are still in rather good agreement with the experimental results.

Knowledge of the phonon band structure is crucial if an accurate calculation of the free energy for the different hydrides is going to be performed. Souvatzis and Eriksson [25] has also calculated the phonon band-structure of αZr using ab initio methods and there results are in very good agreement with the results presented here. In the same way Zhang et al [24] has calculated the phonon band structure for the ϵ-hydride and there results are in agreement with our results. The phonon band structure for γ and δ hydride hasn't been published before and therefore a comparison with our results and previous calculations isn't possible.

In the phonon band structures for the different hydrides a clear band gap of about 100 meV is present. This gap exists because of the large difference in the mass of zirconium and hydrogen atoms. Because zirconium atoms have a larger mass than hydrogen, the vibrational frequencies of zirconium are lower than the vibrational frequencies of the hydrogen atoms and this is the reason for the large band gap in the phonon band structure. This is also evident if we study the phonon partial density of states (PDOS) for the different hydrides, figure 4-6, from which we can draw the conclusion that the low frequency phonons are mainly due to vibrations in the zirconium sublattice, while the high frequency phonons is mainly due to the vibrations among the lighter hydrogen atoms.

In figure 7 the heat capacity at constant volume of αZr and the three different hydrides is seen as a function of the temperature. These heat capacities are calculated from the phonon frequencies of the different compounds. For αZr we have a tabulated value of 25.0866 $JK^{-1}mol^{-1}$ for the heat capacity at

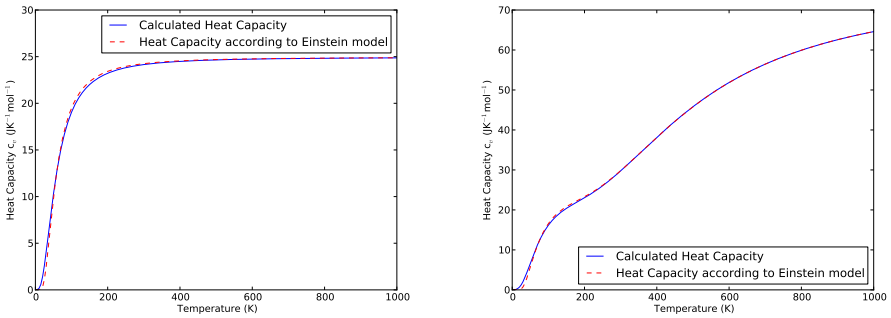

(a) αZr (b) ϵ-ZrH_2

Figure 11: *A comparison between the heat capacity calculated in this work and the heat capacity calculated using the Einstein model for αZr and ϵZrH_2*

room temperature[26]. This is in good agreement with the results obtained from our calculations where a value of $24.15 \mathrm{JK}^{-1}\mathrm{mol}^{-1}$ is obtained.

According to both the Einstein model and the Debye model for the heat capacity of a solid it is given by the Dulong-Petit value of $3R\mathrm{JK}^{-1}\mathrm{mol}^{-1}$ at high temperatures, where R is the ideal gas constant[27]. In the Einstein model [27]a solid is treated as N oscillators with a characteristic frequency ω_E, and the heat capacity in this model is given by:

$$C_v = 3Nk_B \left(\frac{\hbar\omega_E}{k_B T}\right)^2 \frac{e^{\frac{\hbar\omega_E}{k_B T}}}{\left(e^{\frac{\hbar\omega_E}{k_B T}} - 1\right)^2} \tag{26}$$

Despite this simple approach the model can be used to accurately describe the heat capacity of many solids. If we analyse the heat capacities that we have calculated in this work with the Einstein model we see that the heat capacity for αZr very closely resemble that of the ideal Einstein solid. The hydrides on the other hand has a rather peculiar form compared to the ideal heat capacity given by the Einstein model. But as we previous have seen the different hydrides have a large band gap in their phonon band structure. Therefore we can't treat them as a solid with N equivalent oscillators. Instead the hydrides must be treated as solids with two types of oscillator with two different characteristic frequencies. In figures 11(a) and 11(b) a comparison between the heat capacities calculated in this work and the heat capacities calculated using the Einstein model is presented for αZr and the ϵ-hydride. As seen in these figures the Einstein model yields very accurate results for the heat capacities for both αZr and ϵ-hydride. For the γ- and δ-hydrides the

Table 5: *The calculated Einstein frequencies for αZr and the three different hydrides in units of meV*

	$\omega_{E,1}$	$\omega_{E,2}$
α-Zr	15.0	-
γ-ZrH	17.1	152.5
δ-$ZrH_{1.5}$	16.8	147.6
ϵ-ZrH_2	19.5	143.7

Einstein model also yields accurate results. In table 5 the calculated Einstein frequencies for the different hydrides are presented.

The free energy of formation for the different hydrides has been calculated and the result from this calculation is presented in figure 8. The results shows that the ϵ-hydride has the lowest free energy of formation, the δ-hydride has the second lowest free energy of formation and theγ-hydride has the highest free energy of formation. These results are not very surprising since the ϵ-hydride contains more hydrogen than the other two hydrides, allowing it to form more hydrogen bonds and lower the energy more than the other hydrides.

The temperature dependence of the free energy of formation is also not very surprisingly. At low pressures, hydrogen gas has a very high entropy and as the temperature increases the entropy contribution to the free energy of the hydrogen gas increases, lowering the free energy of hydrogen gas as the temperature increases, and therefore at high temperatures the free energy of formation decreases.

The enthalpy of formation for the different hydrides has however a different temperature dependence, at temperatures lower then about 600 K the enthalpy of formation increases as a function of temperature, and at temperatures higher then 600 K the enthalpy of formation is decreasing with temperature. The exact point there the formation enthalpy has its minimum is different for the different hydrides but the overall trend is the same for the different hydrides.

The free energy of formation and enthalpy of formation for the different hydrides are important quantities. But to be able to fully understand the phase stability of the different hydride phases further analysis is required. The most important effect that need to be quantified is the effect that hydrogen in solution has on the free energy of the different compounds. As previously has been noted we have in this work assumed that all hydrogen present in the system will precipitate into one of several very distinct types of hydrides. In reality some hydrogen will remain in solution in the αZr when

hydrides are precipitated. It has previously been shown [21] that a dilute solid solution of Zr-H has a positive formation energy, indicating that it is only entropy effects that stabilize the Zr-H solid solution. Similar effects are very likely to also affect the different hydrides.

8 Conclusion and outlook

From the work presented here several conclusions can be made. First of all the work presented in this thesis has shown that the computer-codes used (ASE/GPAW and phonopy) are very well suited to perform these kind of calculations. Some of the results presented in this work have recently been published ([20],[24]) by others, but the computational methods used by these groups are based on the planewaves-pseudopotential methods, as opposed to the PAW-method used in this work.

In those cases where experimental results and results from other calculations are available, the results in this work is in good agreement with these results. From the calculation of phonon frequencies we can see that the hydrides have two bands of phonon frequencies, corresponding to vibrations in the zirconium and hydrogen sub lattice.

We haven't been able to fully determine the equilibrium hydride phase as a function of temperature and hydrogen content. We can conclude that at intermediate hydrogen concentrations a combination of αZr and a hydride, unclear which one, is the equilibrium structure but at high hydrogen concentrations ϵ-hydride becomes the energetically most favourable.

The work presented in this thesis must be considered to be only a brief introduction to a very interesting subject. There are several possible ways that this work can be continued, one of the most interesting is to calculate the free energy of formation for the different hydrides at different pressure, thereby examining if the equilibrium hydride phase changes if compressive forces are applied. Moreover the effects of hydrogen in solution in the α-matrix and the hydrides must be studied closely before any conclusions about the equilibrium structures at different temperatures and hydrogen concentrations can be made.

Acknowledgement

There are many peoples I would like to thank for helping and encouraging me through the work on this thesis. First of all I would like to thank Anna-Maria Alvarez at Studsvik Nuclear AB for all the help and feedback during the work. Moreover i would like to thank Jakob Blomqvist at Malmö Högskola for his supervision and technical support during the calculations.

I also would like thank the employees at Studsvik Nuclear AB for interesting discussions around the coffee table, and a special thanks to Lotta Nystrand who showed me the running tracks around Studsvik.

Finally I would like to thank my family and friends in Alingsås who has supported me and that always could help me get my mind of things.

References

[1] International Atomic Energy Agency. Delayed hydride cracking of zirconium alloy fuel cladding. Technical Report IAEA-TECDOC-1649, IAEA, 2010.

[2] C.E. Ells. Hydride precipitates in zirconium alloys (a review). *Journal of Nuclear Materials*, 28(2):129 – 151, 1968.

[3] J. Kenneth Shultis and Richard E. Faw. *Fundamentals of Nuclear Science and Engineering*. Marcel Dekker, 2002.

[4] G. Bertolino, G. Meyer, and J. Perez Ipina. Degradation of the mechanical properties of Zircaloy-4 due to hydrogen embrittlement. *Journal of Alloys and Compounds*, 330-332:408–413, 2002.

[5] P. Cotterill. The hydrogen embrittlement of metals. *Progress in Materials Science*, 9(4):205 – 250, 1961.

[6] C.E.Coleman and D. Hardie. The hydrogen embrittlement of α-zirconium - a review. *Journal of Less Common Metals*, 11:168–185, 1966.

[7] E SMITH. The fracture of hydrided material during delayed hydride cracking (DHC) crack-growth. *International Journal Of Pressure Vessels And Piping*, 61(1):1–7, 1995.

[8] E.Zuzek and J.P. Abriata. The H-Zr(Hydrogen-Zirconium) System. *Bulletin of Alloy Phase Diagrams*, 11(4):385–395, 1990.

[9] W.M. Small, J.H. Root, and D. Khatamian. Observation of kinetics of γ zirconium hydride formation in Zr-2.5Nb by neutron diffraction. *Journal of Nuclear Materials*, 256:102–107, 1998.

[10] J.B. Bai and D. Francois. Some evidence of a brittle-ductile transition of zirconium hydride between 20 and 350 ° C. *Journal of Nuclear Materials*, 187:186–189, 1992.

[11] John P. Perdew, Kieron Burke, and Matthias Ernzerhof. Generalized gradient approximation made simple. *Phys. Rev. Lett.*, 77(18):3865–3868, Oct 1996.

[12] K. Parlinski, Z. Q. Li, and Y. Kawazoe. First-principles determination of the soft mode in cubic ZrO_2. *Phys. Rev. Lett.*, 78(21):4063–4066, May 1997.

[13] D. Alfe. Phon: A program to calculate phonons using the small displacement method. *Computer Physics Communications*, 180:2622–2633, 2009.

[14] J. J. Mortensen, L. B. Hansen, and K. W. Jacobsen. Real-space grid implementation of the projector augmented wave method. *Phys. Rev. B*, 71(3):035109, JAN 2005.

[15] S. R. Bahn and K. W. Jacobsen. An object-oriented scripting interface to a legacy electronic structure code. *Comput. Sci. Eng.*, 4(3):56–66, MAY-JUN 2002.

[16] Hendrik J. Monkhorst and James D. Pack. Special points for brillouin-zone integrations. *Phys. Rev. B*, 13(12):5188–5192, Jun 1976.

[17] R Hill. The elastic behaviour of a crystalline aggregate. *Proceedings of the Physical Society. Section A*, 65(5):349, 1952.

[18] Atsushi Togo, Fumiyasu Oba, and Isao Tanaka. First-principles calculations of the ferroelastic transition between rutile-type and $CaCl_2$ -type SiO_2 at high pressures. *Phys. Rev. B*, 78(13):134106, Oct 2008.

[19] S. Yamanaka et al. Characteristics of zirconium hydride and deuteride. *Journal of Alloys and Compounds*, 330–332:99–104, 2002.

[20] Weihua Zhu, Rongshan Wang, Guogang Shu, Ping Wu, and Heming Xiao. First-Principles Study of Different Polymorphs of Crystalline Zirconium Hydride. *Journal of Physical Chemistry C*, 114(50):22361–22368, DEC 23 2010.

[21] C. Domain, R. Besson, and A. Legris. Atomic-scale Ab-initio study of the Zr-H system: I. Bulk properties. *Acta Materialia*, 50:3513–3526, 2002.

[22] K. Niedzwiedz, B. Nowak, and O.J. Zogal. 91Zr NMR in non-stoichiometric zirconium hydrides, ZrHx ($1.55 \leq x \leq 2$). *Journal of Alloys and Compounds*, 194(1):47 – 51, 1993.

[23] E. S. Fisher and C. J. Renken. Single-crystal elastic moduli and the hcp $\rightarrow$ bcc transformation in Ti, Zr and Hf. *Phys. Rev.*, 135(2A):A482–A494, Jul 1964.

[24] Peng Zhang, Bao-Tian Wang, Chao-Hui He, and Ping Zhang. First-principles study of ground state properties of zrh2. *Computational Materials Science*, 50(12):3297 – 3302, 2011.

[25] P. Souvatzis and O. Eriksson. Ab initio calculations of the phonon spectra and the thermal expansion coefficients of the 4*d* metals. *Phys. Rev. B*, 77(2):024110, Jan 2008.

[26] C. Nordling and J. Österman. *Physics Handbook*. Studentlitteratur, 2006.

[27] Charles Kittel. *Introduction to Solid State Physics, 8th ed.* John Wiley & Sons, Inc, 2005.